Journal of Materials Science: Materials in Electronics (2020) 31:7630–7641
https://doi.org/10.1007/s10854-020-03281-2

Effect of Co/Cu partial replacement on fundamental features of Y-123 ceramics

Ozgur Ozturk[1,2] · Abdul R. A. Nefrow[2] · Fatih Bulut[3] · Hakan Ada[4] · Mustafa B. Turkoz[5] · Gurcan Yildirim[6]

Received: 16 January 2020 / Accepted: 20 March 2020 / Published online: 18 April 2020

Abstract

This study is liable for the effect of sample production processes including the standard solid-state reaction (SSR) and classical sol–gel (SG) preparation methods on the fundamental characteristic features, namely electrical, superconducting, crystal structure quality, crystallinity, morphological, strength quality of grain boundary couplings, and interaction between the grains of $YBa_2Cu_{3-x}Co_xO_{7-\delta}$ (Y-123) advanced ceramic compounds within the weight ratio intervals $x = 0$–20%. The main heat treatments are exerted at two main steps: (I) annealing at 950 °C for 24 h in air medium conditions and (II) annealing at 500 °C during 5 h under the oxygen annealing ambient. The standard measurement methods such as powder X-ray diffraction, scanning electron microscopy, energy dispersive spectroscopy, temperature-dependent electrical resistance, and Vickers hardness measurements are performed for the characterization of materials. It is found that the samples prepared at SSR route present much more superior characteristic features as compared to those fabricated at SG technique, being one of the most striking points deduced this work. In more detail, every material prepared crystallizes in the orthorhombic symmetry and exhibits the superconducting nature but considerable decrement in the critical transition temperatures. The onset and offset transition temperatures are noted to decrease regularly from 92.96 K (92.28 K) to 90.20 K (83.59 K); and 90.05 K (90.03 K) to 45.97 K (30.49 K) for the materials prepared by the SSR (SG) route. Similarly, the variation in the lattice cell and average grain size parameters confirm that the Co/Cu substitution damages Y-123 superconducting phase. Additionally, the Co/Cu partial replacement mechanism leads to increase significantly the Vickers hardness results. To sum up, the Co/Cu partial substitution (produced by either SSR or SG method) is plowed to improve the fundamental characteristic features for new, novel, and feasible market application areas of Y-123 cuprate ceramics in the universe economy.

1 Introduction

After the discovery of superconductivity phenomenon on mercury (from the parents of type-I) by Heike Kamerlingh Onnes in the year of 1911 [1], the most crucial improvement for the critical transition temperature was realized in the La–Ba–Cu–O high-temperature ceramic superconductor (member of type-II cuprate-layered perovskite structures with bended Cu–O chains) recorded by Bednorz and Müller scientists in 1986 for the first time. The material exhibited the superconductivity nature at such a temperature of 30 K that is much higher than that of a transition temperature proposed by BCS theorem [2, 3]. When the year indicated 1987, the yttrium transition metal was inserted in the short-range-ordered antiferromagnetic copper-oxide consecutively stacked sheets of rare earth-based Re–Ba–Cu–O high-temperature ceramic superconductors. Thus, new critical transition temperature of YBCO was experimentally observed to be rather higher than the liquid nitrogen temperature [4].

✉ Mustafa B. Turkoz
turkozmb@gmail.com

1 Department of Electrical and Electronics Engineering, Faculty of Engineering and Architecture, Kastamonu University, Kastamonu 37100, Turkey

2 Central Research Laboratory, Kastamonu University, Kastamonu 37100, Turkey

3 Scientific and Technological Research Applications and Research Center, Sinop University, Sinop 57000, Turkey

4 Department of Mechanical Engineering, Faculty of Engineering and Architecture, Kastamonu University, Kastamonu 37100, Turkey

5 Department of Electrical and Electronics Engineering, Faculty of Engineering, Karabuk University, Karabuk 78050, Turkey

6 Department of Mechanical Engineering, Abant Izzet Baysal University, Bolu 14280, Turkey

The discovery enables the superconducting materials much more use in the application fields of motors, transformers, materials engineering, heavy-industrial technology, levitated trains, and industrial energy-related sectors as a consequence of exceeding the thresholds such as the non-toxic, low cost, and easily accessible of liquid nitrogen [5–7]. Throughout the discovery of YBCO cuprate superconducting materials, a number of researchers have extensively studied on the examination and improvement of fundamental characteristic features including the pinning flux mechanism, electrical, superconducting, crystal structure quality, crystallinity, morphological, and strength quality of grain boundary couplings [8]. Besides, one can observe several scientific papers published in the literature on the investigations of superconducting and mechanical performances of Y-123 superconducting crystal system prepared with the different preparation methods, namely the variations in the grinding time, pelletization pressure, calcination, and annealing ambient atmosphere (including environment pressure, time, temperature, and gas atmosphere) dopant type/quantity, chemical composition, doping, addition, and partial substitution in the crystal system [9–15]. The conventional solid-state reaction route (SSR) has commonly been used for the preparation process of poly-crystallized YBCO superconducting ceramic materials. In the technique, the chemical powders (unreactive metal-oxides and carbonates) are exactly weighed and mixed with respect to the certain stoichiometric proportion. The mixture of powder is pressed into a bar within the rectangular or spherical shapes at a certain load value by means of a hydraulic press machine. Then, the solid bars are subjected to the annealing process at a temperature lower than the melting temperature value to provide the superconducting phase. Moreover, the mixture of chemical powder can be multiple ground to increase the homogeneity. However, it is to be mentioned here that the high operating temperature and duration from the preparation methods can damage the stoichiometry and homogeneity of powder chemicals [16]. Recently, the scientists have sometimes preferred the sol–gel material preparation process (one of the wet chemical method) to produce the superconducting ceramic materials due to the simple and low cost. In the method, one or more metal components are dissolved in water or acid to begin the reaction [16].

The critical transition temperature (T_c) is one of the vital characteristic properties for the superconducting compounds. Among the superconducting materials, in the literature the YBCO parents are composed of four main different phases which are abbreviated as Y-123 with the maximum critical transition temperature value of $T_c \approx 92$ K, Y-124 with the T_c of 80 K, Y-247 with the T_c of 40 K and Y-358 with the T_c of 104 K [17, 18]. Therein, the superconducting phases of Y-124 and Y-247 have mostly been studied extensively.

In this study, we try to determine that which preparation procedure (SSR or SG) is much more suitable to produce the Cu-site Co partial substituted Y-123 superconducting phase with higher fundamental characteristic features for the new, novel, and feasible market application areas in the universe economy by means of available characterization methods, namely the powder X-ray diffraction, scanning electron microscopy, energy dispersive spectroscopy, temperature-dependent electrical resistivity, and microhardness investigations.

2 Experimental methods

In this study, the Cu-site Co partial substituted Y-123 cuprate-layered perovskite superconducting samples are prepared by means two different methods: (I) conventional solid-state reaction (SSR) and (II) classical sol–gel routes. The cobalt-nanoparticles within the high purity of about 99.5% (Cobalt powder-325 mesh) are used in both preparation processes. Throughout the former method, the unreactive metal-oxides and carbonates such as Y_2O_3 (Yttrium(III) oxide with the high purity of 99.99%), $BaCO_3$ (Barium carbonate with 99.95%), and CuO (Copper(II) oxide with 99.9995%) are exactly weighed with respect to the stoichiometric ratios (1:2:3) using the electronic balance.

As for the latter preparation method, the acetic acid (Acetic acid glacial, $CH_3CO_2H, \geq 99.85\%$) of 15 mL is used as solvent. Methanol anhydrous (CH_3OH 99.8%) of 15 mL is added to the chemical powder of barium acetate (99.999% trace metals basis, Sigma-Aldrich) with occasional stirring the homogeneous mixture. Then, the yttrium acetate (Yttrium(III) acetate hydrate 99.9% metals basis) is adding to the solution and stirring one more. The additive is thoroughly embedded by stirring in the homogeneous solution. Lastly, both the copper acetate (Copper(II) acetate, 99.99% trace metals basis) and trietanolamin (Tris(2-hydroxyethyl) amine ≥ 99.0) of 8 mL for accelerating dissolution of copper are added into the solution. Besides, the copper acetate is finally added due to its intrinsic quick oxidation characteristic. The solution color turns to turquoise. The last solution is left to stir for the period of 12 h at room temperature in a sealed beaker. Right after, the stirring process remains at the temperature of 80 °C to gel the solution. The gelling solution is heated in a programmable furnace so that the formation of homogeneous solution can change to the powder form. The last products of powder obtained from both the SSR and SG methods are ground in an agate mortar by a pestle for an hour and are exposed to the intermediate-calcination process in a Protherm PLT-120/5 model programmable furnace at 850 °C for 24 h under the normal atmospheric pressure conditions. After the first heat treatment process, each resultant powder is reground two times (totally three times)

in the agate mortar by a pestle for an hour to obtain more and more homogeneity. The mixture of ingredients is pelletized into the rectangular bars by the cold press method. The bars solidified are finally sintered at 930 °C for 24 h in the atmospheric air. With the cooling rate of 5 °C/min the temperature cools down to 500 °C where all the samples are annealed for 5 h under the oxygen annealing ambient. The bulk Cu-site Co replaced cuprate-layered perovskite superconducting compounds prepared with different cobalt content levels of $x = 0.00$, 0.05, 0.10, and 0.20 will thenceforward be abbreviated (with respect to the preparation methods) to be SSR-U, SSR-005, SSR-010, SSR-020, SG-U, SG-005, SGR-010, and SG-020, respectively.

Powder X-ray diffraction patterns of Co/Cu partial substituted Y-123 superconducting materials are examined by a Bruker D8 Advance model X-ray diffractometer using a CuKα target source (1.54 Å) at the medium of air. The experimental diffracted beams are collected in the $2\theta = 3°–90°$ at a scan speed of 4° min^{-1}. Indexation is performed with respect to JCPDS index cards with the JCPD-ICDD (international center for diffraction data) number of 38–1433 using the orthorhombic unit cell. Moreover, the measurements of energy dispersive spectrometry (EDS) and scanning electron microscope (SEM) images at × 2500 magnification are performed in the presence of 10 kV external voltage by use of a FEI Quanta FEG 250 SEM. Additionally, the temperature-dependent resistance measurements for the superconducting materials are measured in the temperature range of 40 K-100 K using the conventional four-probe technique by means of Janis CCS-450 model low temperature electrical measurement system. As for the microhardness tests, the variations of the mechanical performance and mechanical characteristic features belonging to the Cu-site Co partial substituted polycrystalline Y-123 ceramic compounds are searched with the assistant of Vickers hardness measurements performed by SHIMADZU HVM-2 model digital microhardness tester in the test load range of 0.245 N-2.940 N at the room temperature.

3 Results and discussion

3.1 XRD analyses

The powder XRD patterns of pure and Cu-site Co partial substituted Y-123 superconducting ceramic materials are graphically displayed in Fig. 1, where one can see some characteristic Miller indices related to the superconducting phases of YBCO parents. According to the figure, it is obvious that the Y-123 superconducting materials prepared by either SSR and SG preparation methods crystallize in the orthorhombic symmetry. Besides, the figure shows that the widths of characteristic peaks stemmed from the diffracted beams tend to narrow with the increment in the Co/Cu partial substitution level in the Y-123 crystal structure. Similarly, the presence of cobalt impurities in the crystal system damages the characteristic peak intensities. Moreover, it is apparent from the figure that there is no new peak assigned for any impurity or cobalt atoms. In essence, the Co^{+3} foreign inclusions may successfully substitute for the Cu-sites in the Y-123 superconducting crystal structure due to much closer ionic radius. Namely, the ionic radius of a trivalent cation Co^{+3} is 0.745 Å when the ionic radius of a divalent cation Cu^{2+} is 0.730 Å. Thus, the Co^{+3} foreign inclusions prefer to mostly replace for the Cu-sites in the Y-123 crystal system. Stated more succinctly, the increased positive

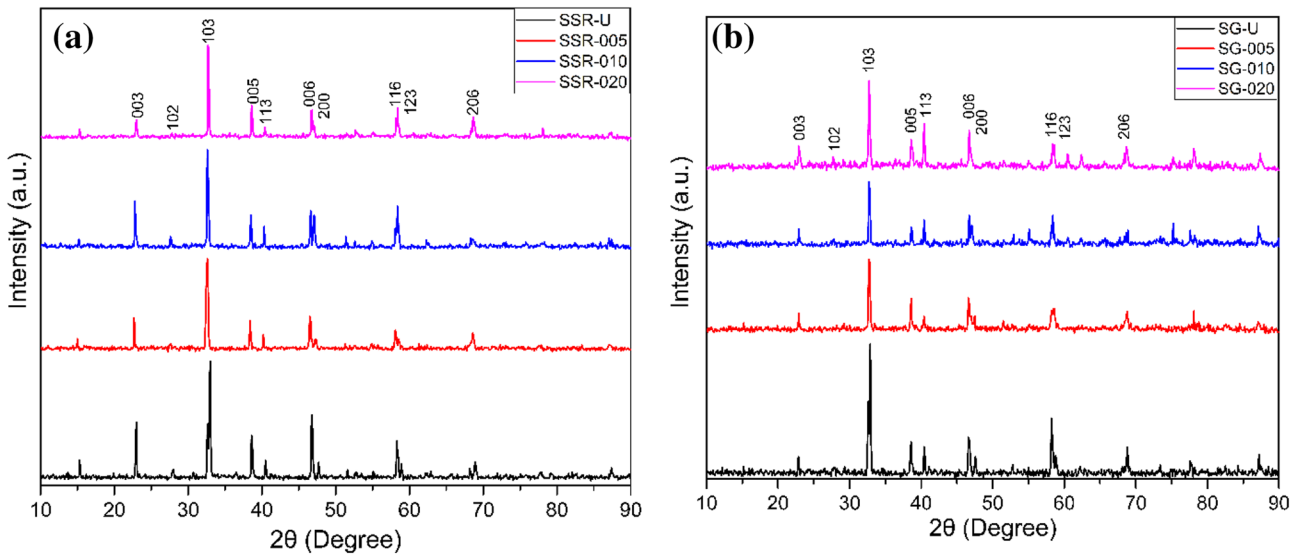

Fig. 1 XRD patterns for the materials prepared by **a** solid-state reaction **b** Sol–gel methods

charge density in the oxygen deficient planes is naturally required to balance with the valency in the Ba–O layers for the charge neutrality. This situation leads directly to prevent the formation of effective and strong electron–phonon coupling probabilities in the superconducting paths driving the superconductivity. Consequently, the superconducting nature is gradually damaged with the enhancement in the Co/Cu partial substitution level.

Further, the XRD patterns show that the characteristics peaks are scarcely affected with the presence of cobalt inclusions in the superconducting matrix. However, the partial replacement of homovalent Co-sites on the Cu-site in the Y-123 crystal system (especially SG method) leads to change in the magnitudes for the main peaks of *103*, *006*, and *003*. This is attributed to the fact that the SG preparation method varies considerably the crystal structure and related characteristic features of Co substituted Cu-site Y-123 solid cuprates. At the same time, the characteristic diffraction peaks in the XRD diffractograms enable us to determine how the Co/Cu partial substitution affects the average grain size and lattice cell parameters founded on the crystal structure. The axis lengths (*a, b*, and *c*) are calculated for the orthorhombic unit cell structure with the aid of distance between plane (abbreviated as *d*) values and (*hkl*) planes given in Eq. 1.

$$\frac{1}{d^2} = \frac{h^2}{a^2} + \frac{k^2}{b^2} + \frac{l^2}{c^2} \tag{1}$$

Similarly, the average crystallite size parameter is calculated by Scherrer–Warren formulas based on the full-width at half maximum [19–21]. Namely,

$$D = 0.941\lambda/B\cos\theta \tag{2}$$

$$B^2 = B_s^2 - B_m^2 \tag{3}$$

in the equations, D is directly related to the crystal thickness, λ is associated with the wavelength for the incident X-rays, Θ presents the Bragg angle, B displays the full width at half maximum depending on the Bragg peak and the abbreviation of B_m is the constant of 0.000007 [22]. All the computations are numerically tabulated in Table 1. In the literature, the lattice cell parameters are arranged as $a = 3.82$Å, $b = 3.88$Å ve $c = 11.68$Å for the standard Y-123 superconducting phase [16]. According to the cell constants given in the table, it is natural to confirm that the axis lengths for every superconducting material prepared by the SSR method is found to be in good agreement with the available data in the literature. Besides, it is to be stressed that the Co/Cu partial substitution changes rarely all the lattice cell parameters. Moreover, the computations in the table show that there is a regular increment trend in the average grain size parameters for all the superconducting samples

Table 1 Average grain size and lattice cell parameters for all the $YBa_2Cu_{3-x}Co_xO_{7-\delta}$ ceramic materials

Sample	D (nm)	a (Å)	b (Å)	c (Å)
SSR-U	29	3.82	3.88	11.68
SSR-005	30	3.82	3.88	11.69
SSR-010	38	3.82	3.88	11.69
SSR-020	43	3.82	3.89	11.68
SG-U	28	3.82	3.86	11.61
SG-005	32	3.74	3.92	11.68
SG-010	33	3.79	3.87	11.74
SG-020	42	3.80	3.87	11.75

(especially the materials produced by the SSR method) as the substitution level enhances up to the maximum content value of $x = 0.20$. All in all, our primary discussion in this part is the fact that the SG method leads to much more vary the lattice cell parameters (with respect to the available literature results) as compared to those of SSR route. Regardless, every result deduced is found to be parallel with the literature results [23, 24].

3.2 SEM and EDS analyses

In this part of paper, we scrutinize the variations in the surface morphology, crystal structure qualities, grain alignment (texturing) distributions, grain boundary coupling problems, connection between the superconducting grains, particle sizes and related distances between the superconducting particles with the aliovalent Co/Cu partial substitution in the $YBa_2Cu_{3-x}Co_xO_{7-\delta}$ ceramic superconducting materials with the assistant of SEM investigations (Figs. 2, Fig. 3). The SEM images are taken using by the Everhart–Thornley Detector (ETD) at × 2500 magnification of secondary electron (SE) image mode in the horizontal field width of 11.7 mm. Additionally, the insets of figures show the same places but at × 10,000 magnification. It is obvious from the micrographs that the surfaces of both the pure samples (especially solid SG-U compound) present porous structure. With the augmentation in the Co/Cu partial replacement level the porosity level is found to degrade considerably. In other words, the existence of cobalt impurity in the Y-123 crystal structure causes to increase the particle sizes in the crystal system. The variation of particle sizes with the substitution presents good agreement with the average grain sizes deduced from XRD patterns. Moreover, one can encounter the positive effects on the grain alignment distributions, grain boundary coupling problems, interaction between the superconducting grains and distances between the superconducting particles with the Co/Cu partial substitution level. In more detail, it would be more precise to confirm that the $YBa_2Cu_{3-x}Co_xO_{7-\delta}$ superconducting materials

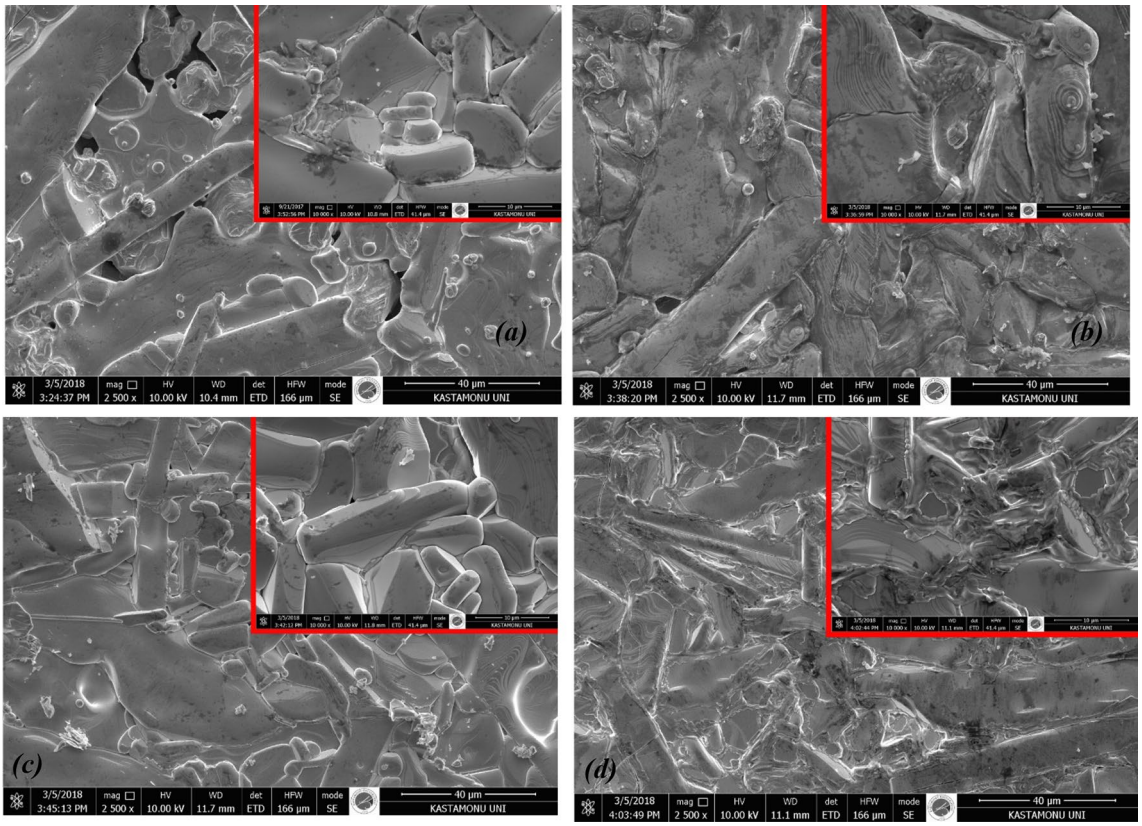

Fig. 2 SEM images for **a** SSR-U, **b** SSR-005, **c** SSR-010, **d** SSR-020 superconducting materials

prepared by the SSR method exhibit much more quality surface morphology (including more uniform surface appearance with the finest connection between superconducting grains, regular grain orientations with lower porosity, larger average grain distribution with the smallest grain boundary coupling problems) as compared to those produced by the SG technique.

As for the EDS results, Figs. 4 and 5 show quantitatively the element distributions of local elemental compositions (only Y, Ba, Cu, Co, and O) in detail. The figures confirm that all the materials are thoroughly prepared with respect to the stoichiometric proportion of $YBa_2Cu_{3-x}Co_xO_{7-\delta}$ ceramic materials. It is clear from the figures that the atomic distributions of Y, Ba, and O remain approximately constant for all the superconducting materials. Conversely, the Co atomic distributions are noted to ascend systematically with increment in the distributions of substitution atom (Cu) in the Y-123 superconducting matrix as planned. This is in association with the fact that the cobalt foreign atoms may mostly be replaced successfully by the Cu-sites in the Y-123 crystal lattice. Stated more succinctly, the EDS surveys verify why the fundamental characteristic features change harshly based on both the preparation method and cobalt concentration level.

3.3 Electrical resistance examination

Temperature-dependent electrical resistance results allow the researchers to provide some characteristic behaviors at relativistic low temperatures. Figure 6 demonstrates the dc electrical resistance results for the $YBa_2Cu_{3-x}Co_xO_{7-\delta}$ superconducting materials over the temperature range of 40 K-100 K. According to the figure, the existence of Co^{3+} ions in the Y-123 crystal system affects extremely the fundamental electrical and superconducting properties. On this basis, the practical consequence is that the cobalt inclusions successfully incorporate into the Y-123 superconducting crystal matrix. It is apparent from Fig. 6 that the critical transition temperature (T_c) values are found to decrease with the enhancement in the Co/Cu partial substitution level. However, all the materials exhibit the superconducting nature due to the maintaining of orthorhombic symmetry in the crystal structures. One can see some superconducting characteristics such as the onset critical transition (T_c^{onset}), offset critical transition temperature (T_c^{offset}) and degree of broadening ($\Delta T_C = T_c^{\text{onset}} - T_c^{\text{offset}}$) parameters in Table 2. It is obvious form the table that the bulk pure samples (SSR-U and SG-U compounds) show the highest critical transition temperature values (T_c^{onset} and T_c^{offset}) whereas the minimum

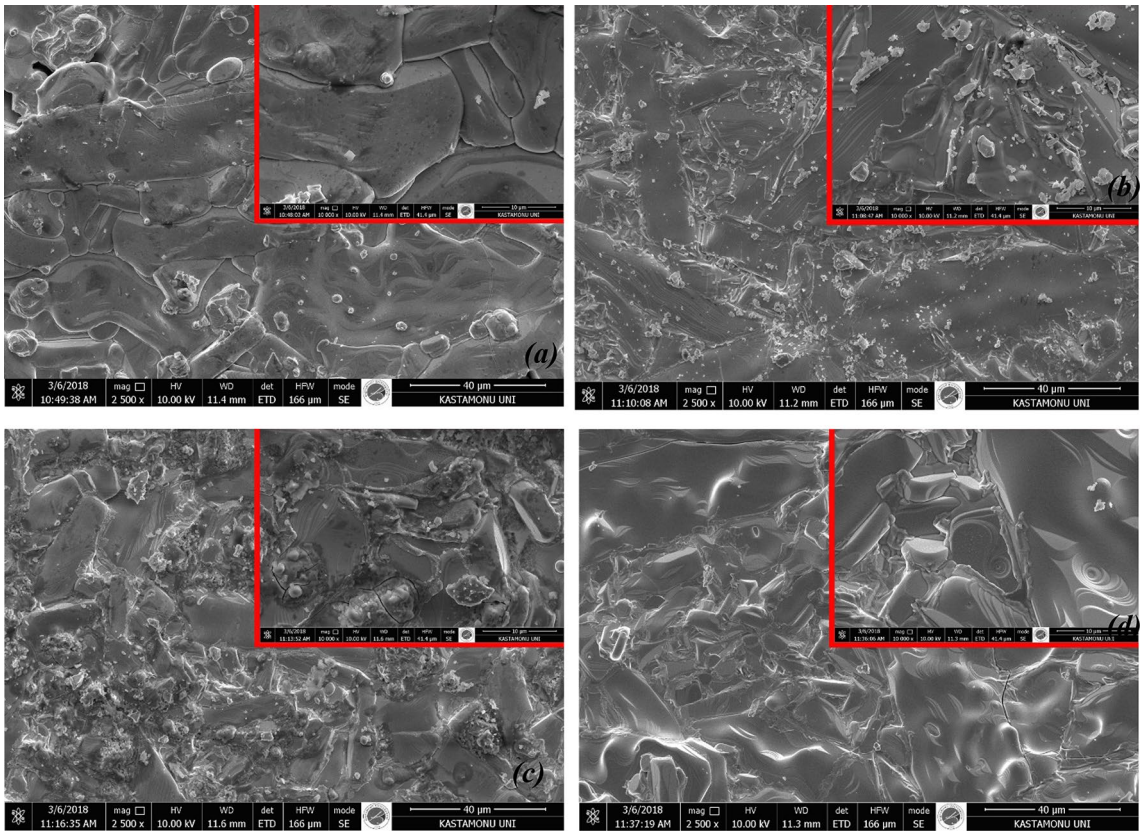

Fig. 3 SEM pictures for **a** SG-U, **b** SG-005, **c** SG-010, **d** SG-020 superconductors

ΔT_C parameters are also observed for these materials among the compounds prepared in this work. In this respect, the existence of cobalt impurities instead of copper ions damages considerably the formation of effective and strong electron–phonon coupling probabilities (homogenous clusters) in the superconducting paths [25]. In other words, the cobalt ions lead to localize the densities of active and dynamic electronic states at Fermi energy level in the Y-123 crystal matrix [26, 27]. To sum up, the mobile hole carrier concentration diverges from the optimum value in the effective and active Cu–O_2 consecutively stacked sheets of adjacent superconductive layers in the hole-induced Y-123 materials, and thus the superconducting nature degrades rapidly with the Co/Cu partial substitution level.

As for the comparison between the experimental measurement results, the critical transition temperatures of $YBa_2Cu_{3-x}Co_xO_{7-\delta}$ ceramic materials prepared by SG method are found to rather lower than those of superconducting materials produced by the SSR technique. In this regard, the smallest parameters are observed to be 30.49 K and 45.97 K for the bulk SG-20 and SSR-20 materials, respectively. The maximum T_c^{onset} and T_c^{offset} values of 92.96 K and 90.05 K ascribes to the SSR-U compound. On the other hand, the minimum value of ΔT_C is found to be about 2.25 K for the SG-U sample. With the enhancement in the Co/Cu partial substitution level the value is noted to more and more increase towards the global maximum values of 44.23 K and 53.10 K for the SG-20 and SSR-20 superconducting materials, respectively.

Further, the room temperature resistance is the crucial electrical feature of materials. According to the graphics in Fig. 6, the room temperature resistance tends to increase gradually with enhancing the Co/Cu partial substitution level in the Y-123 crystal structure due to the rapid augmentation in the permanent structural defects, porosity, disorders in orientation of adjacent layers and grain boundary coupling problems [28–32]. It is to be mentioned here that the Cu-site Co partial substituted Y-123 inorganic ceramics prepared by the SG method exhibit much more resistance values in comparison with the resistances of the compounds produced by the SSR technique. The findings are totally supported by the experimental results deduced from the XRD examinations. It is another probable result inferred from the figure that there seems to be the pseudo-transitions in the SSR-010, SSR-020, and SG-020 materials. This is attributed to the presence of impurity over the grain boundaries, leading to the boundary weak-links in the crystal lattice [33].

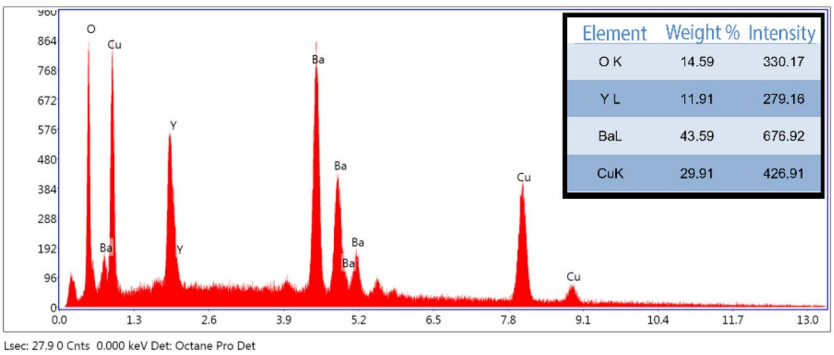

(a)

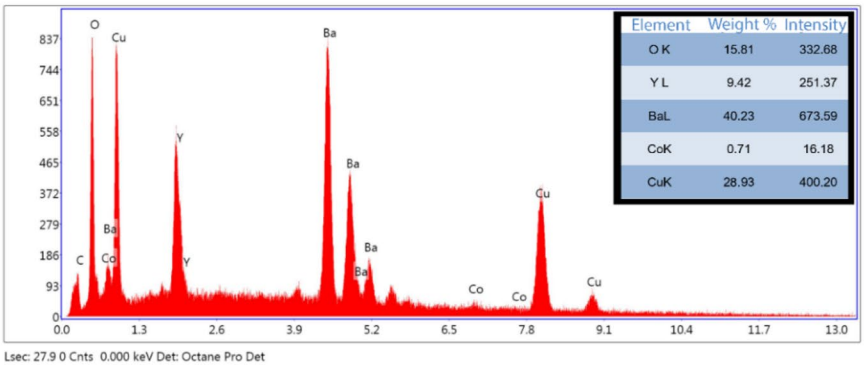

(b)

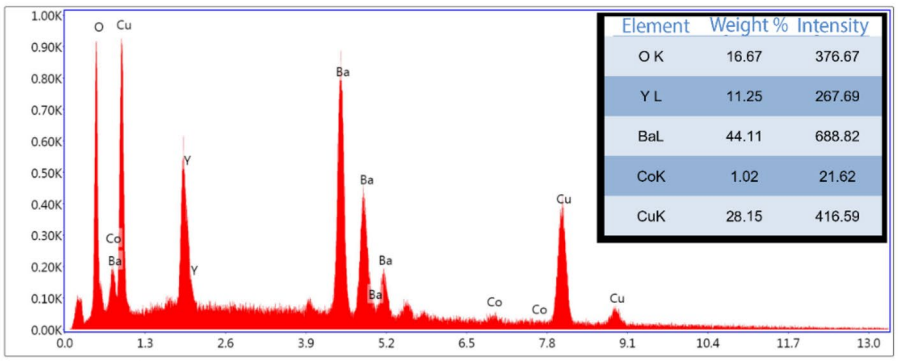

(c)

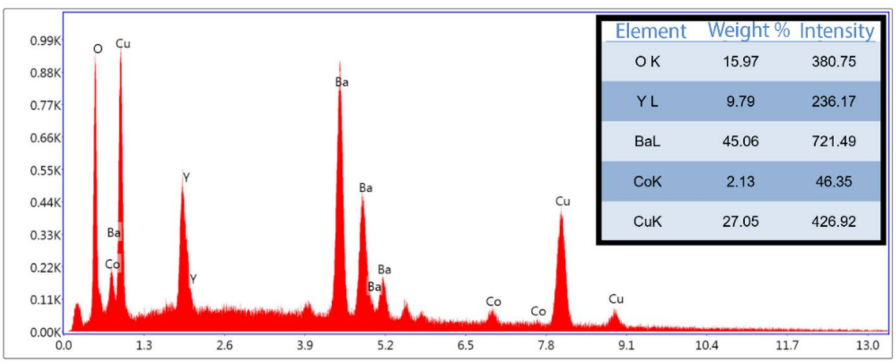

(d)

Fig. 4 EDS results for **a** SSR-U, **b** SSR-005, **c** SSR-010, **d** SSR-020 superconducting samples

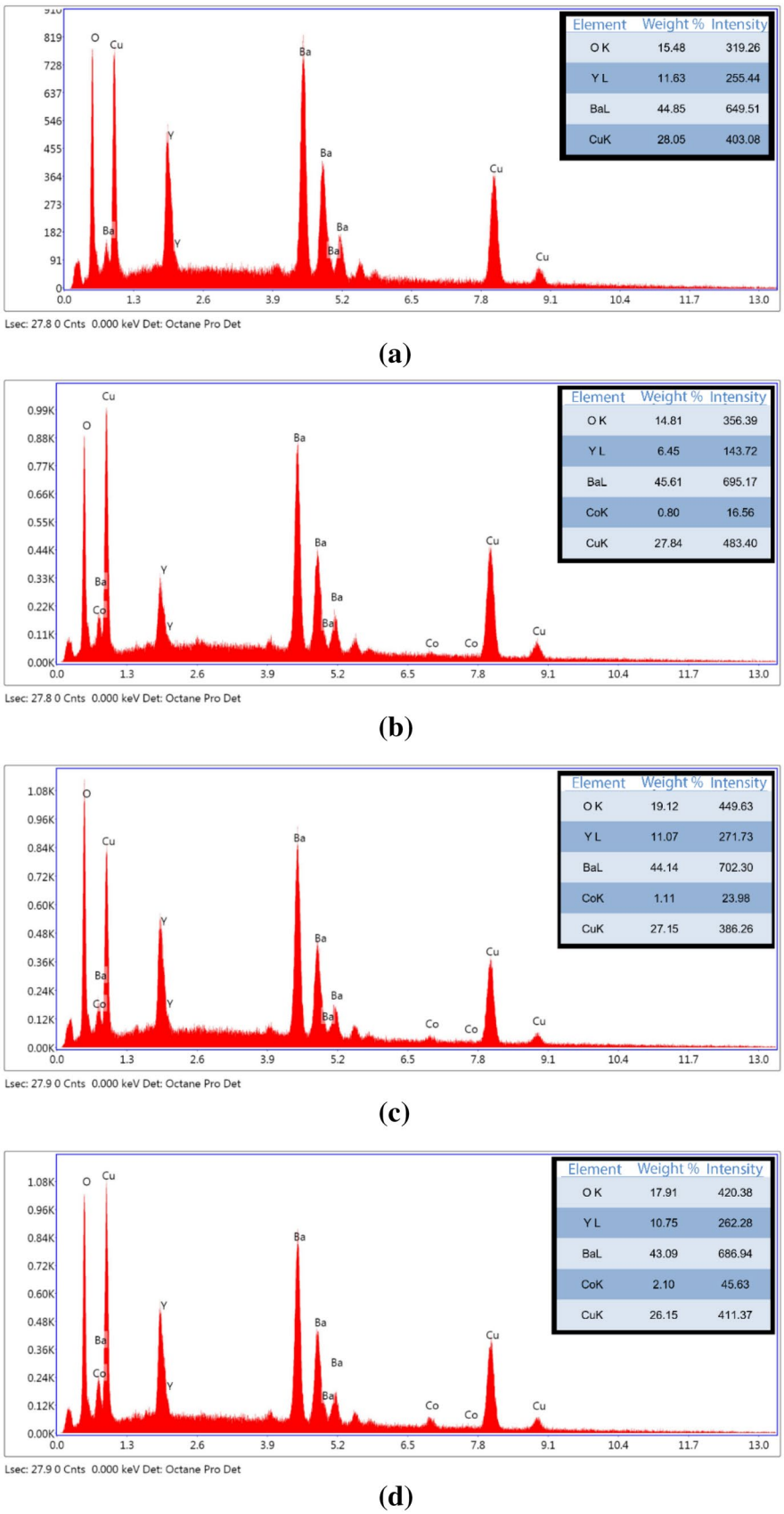

Fig. 5 EDS results for **a** SG-U, **b** SG-005, **c** SG-010, **d** SG-020 superconductors

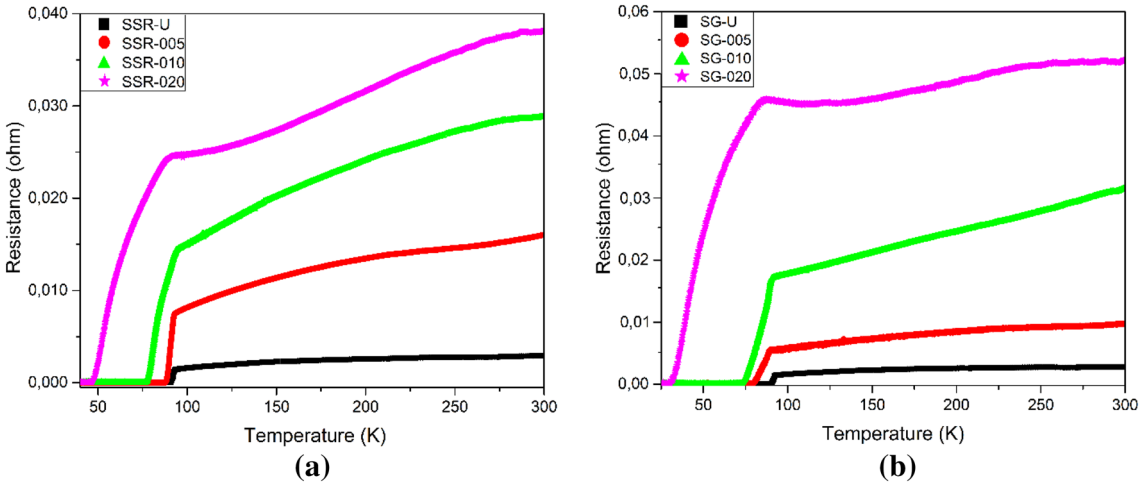

Fig. 6 Temperature-dependent electrical resistance measurements for the materials prepared by **a** solid-state reaction **b** Sol–gel methods

Table 2 Superconducting characteristic parameters deduced from temperature-dependent electrical resistance measurements

Sample	Critical temperature (K)		ΔT_C(K)
	T_C^{onset}	T_C^{offset}	T_C^{onset}-T_C^{offset}
SSR-U	92.96	90.05	2.91
SSR-005	92.72	87.91	4.81
SSR-010	92.6	76.74	15.86
SSR-020	90.2	45.97	44.23
SG-U	92.28	90.03	2.25
SG-005	89.09	79.38	9.71
SG-010	89.05	72.71	16.34
SG-020	83.59	30.49	53.1

3.4 Microhardness researches

Besides the superconducting properties, the mechanical performance and mechanical characteristics play an important role on the potential usages in the application fields such as the industrial, technological, materials science engineering, potential metallurgical, and energy technology of superconducting ceramic materials [27–36]. In this respect, the optimizations of some mechanical performance features, namely the elastic modulus, impact resistance, stiffness, mechanical durability, fracture toughness, yield strength, flexural strength, elastic stiffness coefficient, and brittleness index parameters, are of some importance. For this aim, the scientists have used a number of methods including Brinell, Rockwell, Knoop, and Vickers hardness tests. Therein, the Vickers hardness measurement method has commonly been used for the characteristic examination of ceramic superconducting materials due to the inherit several advantages: simple, low cost, fast, reliable, small indentation trace, non-destructive, etc.[37, 38]. The hardness parameter being directly related to the resistant against the applied external load can be changed in terms of material preparation methods. The information about the mechanical characterization of a material is obtained from the microhardness tests depending on the distance measurement between indentation diagonals (on the specimen surfaces) stemmed from various applied indentation test load intervals 0.245 N-2.940 N for loading time of 10 s. The Vickers hardness (H_v) parameters are calculated from the following equation:

$$H_V = 1854.4\left(\frac{F}{d^2}\right) \tag{4}$$

here F shows the external test load applied on the surface when d provides the average of indentation diagonal lengths. The test results also enable us to determine the elastic modulus (E), yield strength (Y), and fracture toughness (K_{IC}) parameters belonging to all the polycrystalline $YBa_2Cu_{3-x}Co_xO_{7-\delta}$ cuprate superconductors prepared in this work [39].

$$E = 81.9635H_V \tag{5}$$

$$Y \approx H_V/3 \tag{6}$$

$$K_{IC} = \sqrt{2E\gamma} \tag{7}$$

in Eq. 7, γ points out the surface energy value resulted from the notches during the indentation process. The differentiations of Vickers hardness parameters as a function of external test loads for every material produced in this study are graphically displayed in Fig. 7 when the variations of microhardness, elastic modulus, yield strength, and fracture toughness parameters against the applied indentation test loads are numerically listed in Table 3 in detail. It is obvious from the figure that the Vickers hardness parameters (for all

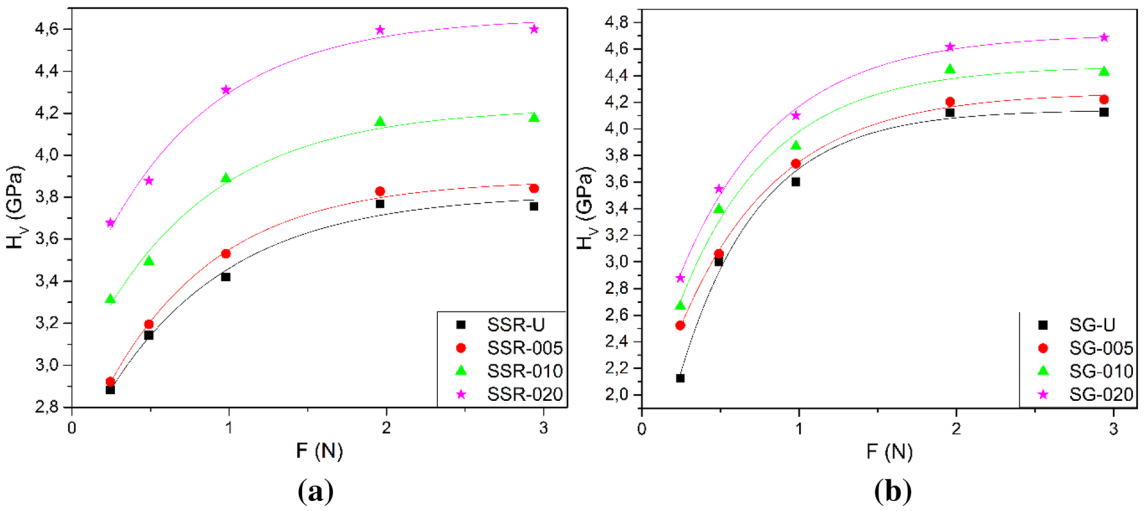

Fig. 7 Variation of Vickers hardness parameters with applied test loads for the $YBa_2Cu_{3-x}Co_xO_{7-\delta}$ (Y-123) cuprate-layered perovskite superconducting materials prepared by **a** solid-state reaction **b** Sol–gel methods

the materials prepared by either the SSR or SG methods) tend to increase with the Co/Cu partial substitution level up to the maximum dopant level of $x = 0.20$. On this basis, the SSR-020 and SG-020 materials exhibit the maximum microhardness values at any applied test loads. Furthermore, the Vickers hardness parameters are found to enhance constantly with the increment in the applied indentation test loads as a consequence of unusual reverse indentation size effect related to the non-linear increase with ascending the external test load [40–42]. However, the materials prepared by the SG method exhibit far higher Vickers hardness values as compared to those of compounds produced by the SSR route. According to the combination results of preparation method and applied test load, the highest microhardness value of 4.688 GPa is observed for the bulk SG-020 superconducting compound at the applied test load of 2.940 N. Finally, the saturation limit regions are found to be about 1 N for all the materials. Figure 7 guarantees that especially the SG-U material most easily reaches its saturation limit value among the materials.

4 Conclusion

In this study, the $YBa_2Cu_{3-x}Co_xO_{7-\delta}$ (Y-123) cuprate-layered perovskite superconductors within the weight ratio of $x = 0$–20% are produced by the standard solid-state reaction and classical sol–gel methods. The variations of fundamental characteristic features are investigated by the available measurement methods such as XRD, SEM, EDS, R-T, and Vickers hardness examinations. All the experimental (particularly EDS surveys) results indicate that the Co^{+3} impurities may mostly substitute for the Cu-sites in the Y-123 superconducting crystal structure. The XRD results show that the aliovalent Co/Cu nano-particle substitution damages hardly any the orthorhombic symmetry and lattice cell parameters due to closer ionic radius values. In this respect, every compound produced by the SSR method obtains nearly 3.82 Å for *a* lattice cell constant, 3.88–3.89 Å for *b* lattice parameter and 11.68–11.69 Å for *c*-axis length. However, it is noted that there is a relatively high deviation in the lattice cell parameters of samples prepared by the SG method. Namely, *a, b* and *c* lattice parameters are found to be in a range 3.74–3.80 Å, 3.86–3.92 Å, and 11.61–11.75 Å, respectively. Moreover, the average grain size parameters are found to increase systematically from 28.95 (28.21) nm to 43.28 (41.81) nm for the Y-123 compounds prepared by the SSR (SG) method with the enhancement in the substitution level. As for the SEM images, the porosity level is observed to diminish remarkably with the augmentation in the Co/Cu partial replacement level in the Y-123 crystal system due to the improvement in the grain alignment distributions, particle sizes, grain boundary couplings and connection between the superconducting grains. Besides, the samples produced by the SSR method present much more quality surface morphology as compared to those produced by the SG technique. Additionally, the electrical resistance measurements figure out that the T_c^{onset} and T_c^{offset} values reduce gradually from 92.96 K until 90.20 K; and 90.05 K to 45.97 K for the materials prepared by the SSR route with the augmentation of Co/Cu partial substitution level while the parameters are found to be in a range of 92.28–83.59 K and 90.03–30.49 K for the materials prepared by the SG method, respectively. Thus, the mobile hole carrier concentration diverges from the optimum value, and the superconducting nature degrades remarkably. At the same time, the Vickers

Table 3 Evaluated H_V, E, Y and K_{IC} values for every material at different applied test loads

Sample	F (N)	H_V (GPa)	E(GPa)	Y(GPa)	$K_{IC} \times 10^2$ (Pa/m$^{1/2}$)
SSR-U	0.245	2.881	236.15	0.960	− 210.218
	0.490	3.143	257.63	1.048	− 219.569
	0.980	3.420	280.28	1.140	− 229.04
	1.960	3.768	308.80	1.256	− 240.411
	2.940	3.755	307.80	1.252	− 239.996
SSR-005	0.245	2.922	239.47	0.974	− 141.84
	0.490	3.195	261.87	1.065	− 140.349
	0.980	3.530	289.31	1.177	− 137.575
	1.960	3.828	313.75	1.276	− 134.477
	2.940	3.841	314.84	1.280	− 135.382
SSR-010	0.245	3.313	271.51	1.104	− 151.091
	0.490	3.492	286.23	1.164	− 148.488
	0.980	3.887	318.59	1.296	− 146.139
	1.960	4.157	340.73	1.386	− 142.642
	2.940	4.175	342.20	1.392	− 143.498
SSR-020	0.245	3.677	301.37	1.226	− 191.1
	0.490	3.878	317.83	1.293	− 187.469
	0.980	4.311	353.34	1.437	− 182.615
	1.960	4.597	376.77	1.532	− 177.848
	2.940	4.601	377.12	1.534	− 176.929
SG-U	0.245	2.126	174.25	0.709	− 281.652
	0.490	3.073	251.87	1.024	− 338.62
	0.980	3.601	295.15	1.200	− 366.558
	1.960	4.122	337.85	1.374	− 392.18
	2.940	4.126	338.18	1.375	− 392.37
SG-005	0.245	2.523	206.77	0.841	− 241.036
	0.490	3.031	248.45	1.010	− 227.791
	0.980	3.638	298.16	1.213	− 219.388
	1.960	4.204	344.59	1.401	− 210.46
	2.940	4.221	345.93	1.407	− 211.011
SG-010	0.245	2.668	218.66	0.889	− 240.404
	0.490	3.394	278.19	1.131	− 230.928
	0.980	3.868	317.02	1.289	− 219.256
	1.960	4.445	364.37	1.482	− 213.717
	2.940	4.427	362.88	1.476	− 215.115
SG-020	0.245	2.881	236.15	0.960	− 264.164
	0.490	3.548	290.83	1.183	− 245.063
	0.980	4.100	336.07	1.367	− 239.564
	1.960	4.616	378.36	1.539	− 231.789
	2.940	4.688	384.24	1.563	− 231.975

hardness experimental results show that the hardness parameters enhance constantly with the increment in the Co/Cu partial substitution level. Especially, the superconducting materials prepared by the SSR method exhibit rather smaller microhardness parameters as compared to those of compounds produced by the SG route. Moreover, the mechanical curves display that the saturation limit regions are found to be about 2 N for all the samples studied, and the SG-U material reaches most rapidly its saturation limit value. Also, it is to be declared here that all the compounds exhibit the *RISE* behavior.

Acknowledgment The authors would like to thank the Kastamonu University Research and Application Center for supports.

References

1. H.K. Onnes.: Springer Netherlands, Dordrecht. 264–266 (1991)
2. J.G. Bednorz, K.A. Müller, Z. Für Phys. **64**, 189–193 (1986)
3. A. Harabor, P. Rotaru, N.A. Harabor, P. Nozar, A. Rotaru, Ceram. Int. **45**, 2899–2907 (2019)
4. M.K. Wu, J.R. Ashburn, C.J. Torng, P.H. Hor, R.L. Meng, L. Gao, Z.J. Huang, Y.Q. Wang, C.W. Chu, Phys. Rev. Lett. **58**, 908–910 (1987)
5. Y. Zalaoglu, B. Akkurt, M. Oz, G. Yildirim, J. Mater. Sci. **28**, 12839–12850 (2017)
6. B. Akkurt, G. Yildirim, J. Mater. Sci. **27**, 13034–13043 (2016)
7. S.B. Guner, Y. Zalaoglu, T. Turgay, O. Ozyurt, A.T. Ulgen, M. Dogruer, G. Yildirim, J. Alloys Compd. **772**, 388–398 (2019)
8. A.T. Ulgen, T. Turgay, C. Terzioglu, G. Yildirim, M. Oz, J. Alloys Compd. **764**, 755–766 (2018)
9. F.B. Azzouz, M. Zouaoui, K.D. Mani, M. Annabi, G.V. Tendeloo, M.B. Salem, Phys. C Supercond. **442**, 13–19 (2006)
10. N. Güçlü, U. Kölemen, O. Uzun, S. Çelebi, Phys. C Supercond. **433**, 115–122 (2005)
11. J.J. Roa, E. Jiménez-Piqué, X.G. Capdevila, M. Segarra, J. Eur. Ceram. Soc. **30**, 1477–1482 (2010)
12. A. Öztürk, I. Düzgün, S. Çelebi, J. Alloys Compd. **495**, 104–107 (2010)
13. S. Dadras, S. Dehghani, M. Davoudiniya, S. Falahati, Mater. Chem. Phys. **193**, 496–500 (2017)
14. D. Volochová, S. Piovarči, M. Radušovská, V. Antal, J. Kováč, K. Jurek, M. Jirsa, Phys. C Supercond. **494**, 36–40 (2013)
15. D. Volochova, K. Jurek, M. Radusovska, S. Piovarci, V. Antal, J. Kovac, M. Jirsa, P. Diko, Phys. C Supercond. **496**, 14–17 (2014)
16. L.M. Yeoh, M. Ahmad, J. Non. Cryst. Solids. **354**, 4012–4018 (2008)
17. S. Bolat, S. Kutuk, J. Supercond. Nov. Magn. **25**, 731–738 (2012)
18. A. Aliabadi, Y. Akhavan Farshchi, M. Akhavan, Phys C Supercond **69**, 2012–2014 (2009)
19. M. Ahmadipour, M.F. Ain, Z.A. Ahma, J. Mater. Sci. **28**, 12458–12466 (2017)
20. L. Zhang, S. Du, Y. Liu, P. Zheng, X. Yuan, J. Huang, S. Guo, Micro. Nano Lett. **11**, 147–157 (2016)
21. M. Ahmadipour, N.A. Rejab, M.F.A. Rahman, M.F. Ain, A. Ahmad, Ceram. Int. **44**, 6904–6911 (2018)
22. C. Terzioglu, M. Yilmazlar, O. Ozturk, E. Yanmaz, Phys. C Supercond. **423**, 119–126 (2005)
23. N.Y. Erwana, A.N. Jannah, N.A. Jamion, J. Acad. **6**, 31–38 (2018)
24. M.M. Dihom, A.H. Shaari, H. Baqiah, N.M. Al-Hada, C.S. Kien, R.S. Azis, M.M.A. Kechik, Z.A. Talib, R. Abd-Shukor, Results Phys. **7**, 407–412 (2017)
25. Y. Zalaoglu, F. Karaboga, C. Terzioglu, G. Yildirim, Ceram. Int. **43**, 6836–6844 (2017)
26. N.K. Saritekin, M. Pakdil, G. Yildirim, M. Oz, T. Turgay, J. Mater. Sci. Electron. **27**, 956–965 (2016)
27. P.B. Allen, W.E. Pickett, H. Krakauer, Phys. Rev. B. **37**, 7482–7490 (1988)
28. Y. Slimani, E. Hannachi, M.K.B. Salem, A. Hamrita, A. Varilci, W. Dachraoui, Phys. B **450**, 7–15 (2014)

29. S. Martin, M. Gurvitch, C.E. Rice, A.F. Hebard, P.L. Gammel, R.M. Fleming, A.T. Fiory, Phys. Rev. B. **39**, 9611–9613 (1989)
30. R. Shabna, P.M. Sarun, S. Vinu, U. Syamaprasad, J. Alloys Compd. **493**, 11–16 (2010)
31. D.M. Newns, P.C. Pattnaik, C.C. Tsuei, Phys. Rev. B. **43**, 3075–3084 (1991)
32. Y. Zalaoglu, G. Yildirim, C. Terzioglu, J. Mater. Sci. Mater. Electron. **24**, 239–247 (2013)
33. B.D. Josephson, Possible new effects in superconductive tunnelling. Phys. Lett. **1**, 251–253 (1962)
34. H. Miao, M. Meinesz, B. Czabaj, J. Parrell, S. Hong, U. B. Balachandran, K. Amm, D. Evans, E. Gregory, P. Lee, M. Osofsky, S. Pamidi, C. Park, J. Wu, M. Sumption. AIP Conference Proceedings, pp. 423–430 (2008)
35. RK Werner Buckel, *Superconductivity: Fundamentals and Applications*, 2ndnd Revised edn. (Wiley-VCH, Weinheim, 2004)
36. H.H. Xu, L. Cheng, S.B. Yan, D.J. Yu, L.S. Guo, X. Yao, J. Appl. Phys. **111**, 103910 (2012)
37. M.M. Ibrahim, S.M. Khalil, A.M. Ahmed, J. Phys. Chem. Solids. **61**, 1553–1560 (2000)
38. R. Awad, A. Abou-Aly, M.M.H.A. Gawad, I.-G. Eldeen, I. G-Eldeen. J. Supercond. Nov. Magn. **25**, 739–745 (2012)
39. M. Dogruer, G. Yildirim, O. Ozturk, A. Varilci, N. Soylu, O. Gorur, C. Terzioglu, J. Mater. Sci. **24**, 1264–1273 (2013)
40. M.B. Turkoz, S. Nezir, O. Ozturk, E. Asikuzun, G. Yildirim, C. Terzioglu, A. Varilci, J. Mater. Sci. **24**, 2414–2421 (2013)
41. J. Gong, Y. Li, J. Mater. Sci. **35**, 209–213 (2000)
42. O. Ozturk, E. Asikuzun, S. Kaya, N.S. Koc, M. Erdem, J. Supercond. Nov. Magn. **30**, 1161–1169 (2017)